SANDIA REPORT
SAND2014-17881
Unlimited Release
Printed September, 2014

Proposed Testing to Assess the Accuracy of Glass-To-Metal Seal Stress Analyses

Robert S. Chambers, John M. Emery, Rajan Tandon, Bonnie R. Antoun, Mark E. Stavig, Clay Newton, Cory Gibson and Denise Bencoe

Prepared by
Sandia National Laboratories
Albuquerque, New Mexico 87185 and Livermore, California 94550

Sandia National Laboratories is a multi-program laboratory managed and operated by Sandia Corporation, a wholly owned subsidiary of Lockheed Martin Corporation, for the U.S. Department of Energy's National Nuclear Security Administration under contract DE-AC04-94AL85000.

Approved for public release; further dissemination unlimited.

Sandia National Laboratories

Issued by Sandia National Laboratories, operated for the United States Department of Energy by Sandia Corporation.

NOTICE: This report was prepared as an account of work sponsored by an agency of the United States Government. Neither the United States Government, nor any agency thereof, nor any of their employees, nor any of their contractors, subcontractors, or their employees, make any warranty, express or implied, or assume any legal liability or responsibility for the accuracy, completeness, or usefulness of any information, apparatus, product, or process disclosed, or represent that its use would not infringe privately owned rights. Reference herein to any specific commercial product, process, or service by trade name, trademark, manufacturer, or otherwise, does not necessarily constitute or imply its endorsement, recommendation, or favoring by the United States Government, any agency thereof, or any of their contractors or subcontractors. The views and opinions expressed herein do not necessarily state or reflect those of the United States Government, any agency thereof, or any of their contractors.

Printed in the United States of America. This report has been reproduced directly from the best available copy.

Available to DOE and DOE contractors from
U.S. Department of Energy
Office of Scientific and Technical Information
P.O. Box 62
Oak Ridge, TN 37831

Telephone: (865) 576-8401
Facsimile: (865) 576-5728
E-Mail: reports@adonis.osti.gov
Online ordering: http://www.osti.gov/bridge

Available to the public from
U.S. Department of Commerce
National Technical Information Service
5285 Port Royal Rd.
Springfield, VA 22161

Telephone: (800) 553-6847
Facsimile: (703) 605-6900
E-Mail: orders@ntis.fedworld.gov
Online order: http://www.ntis.gov/help/ordermethods.asp?loc=7-4-0#online

SAND2014-17881
Unlimited Release
Printed September, 2014

Proposed Testing to Assess the Accuracy of Glass-To-Metal Seal Stress Analyses

Robert S. Chambers and John Emery
Component Science & Mechanics

Rajan Tandon
Materials Reliability

Bonnie R. Antoun
Mechanics of Materials

Mark E. Stavig
Organic Materials Science

Clay Newton and Cory Gibson
Materials Reliability

Denise Bencoe
Advanced Materials Laboratory

Sandia National Laboratories
P.O. Box 5800
Albuquerque, New Mexico 87185-MS0346

Abstract

The material characterization tests conducted on 304L VAR stainless steel and Schott 8061 glass have provided higher fidelity data for calibration of material models used in Glass-To-Metal (GTM) seal analyses. Specifically, a Thermo-Multi-Linear Elastic Plastic (thermo-MLEP) material model has been defined for SS304L and the Simplified Potential Energy Clock nonlinear viscoelastic model has been calibrated for the S8061 glass. To assess the accuracy of finite element stress analyses of GTM seals, a suite of tests are proposed to provide data for comparison to model predictions.

ACKNOWLEDGMENTS

The authors would like to thank Ryan Jamison for reviewing this document. We also would like to thank Brian Werner for his digital image correlation (DIC) work.

Table of Contents

Proposed Testing to Assess the Accuracy of Glass-To-Metal Seal Stress Analyses 3

Acknowledgments 4

Figures 6

Tables 7

1 Introduction 9

2 GTM Seal Validation Testing 11

2.1 Indentation Tests to Infer Stresses from Crack Patterns 11

2.2 Measuring Perturbations in the Ambient State of the Concentric Compression Glass Seal 15

2.3 Bi-material GTM Deformations 18

2.4 Digital Image Correlation (DIC) Methods 20

3 Some Unexpected discovery 23

4 Summary 25

6 References 27

7 Appendix A: Legacy material properties 29

8 Appendix B: Revised material properties 8/1/14 33

Distribution 39

FIGURES

Figure 1 Finite element mesh of concentric, single-pin Glass-To-Metal seal 9
Figure 2 Concentric GTM seal with indentations on surface of the S8061 glass..... 12
Figure 3 Higher resolution picture of the glass microstructure and cracking at indentations 13
Figure 4 Comparison of vertical cracks generated in indentations on S8061 glass from annealed and quenched concentric GTM seals 14
Figure 5 Comparison of horizontal cracks generated in indentations on S8061 glass from annealed and quenched concentric GTM seals 15
Figure 6 Strain gauge on shell of concentric GTM seal proposed for validation test (thermal cycling, boring through glass or cutting shell)..... 16
Figure 7 Finite element mesh of concentric seal for cutting..... 17
Figure 8 Hoop strain data and FEA predictions obtained using legacy material models to simulate cutting through the shell in a concentric GTM seal 17
Figure 9 Hoop strain data and legacy predictions for shell cutting process in concentric GTM seal assuming glass-shell contact with a friction coefficient equal to 0.60 18
Figure 10 Picture of bi-material beam made from SS304L VAR and S8061 glass showing deformed shape room temperature (glass on top)..... 19
Figure 11 Room temperature deflected shapes from GTM bi-material beams compared to finite element analysis predictions based on two property sets, legacy and newly calibrated thermo-MLEP and SPEC models 20
Figure 12 Photographs of concentric seal before and after application of the speckle pattern for the digital image correlation study..... 21
Figure 13 Painted contour of DIC first principal strain change from RT to T=102 °C..... 21
Figure 14 Painted contour of DIC first principal strain change from RT after heating then cooling to 2 °C 22
Figure 15 Plots of temperature dependent hardening functions in Adagio thermoelastic plastc model for SS304L VAR 36

TABLES

Table 1 SPEC model parameters for Schott 8061 glass 37
Table 2 Prony series coefficients fit to tan delta from second torsion test 37

1 INTRODUCTION

Glass-To-Metal (GTM) seals are used to provide electrical connections to components that must be hermetically sealed. In a typical application, electrical connectivity is provided through metallic pins arranged within an opening of a metallic shell that is sealed with a glass to insulate/isolate the pin from the housing. During the sealing process, the glass is heated to its working point to allow it to flow, filling the voids between the pin and the housing. Then the entire assembly is cooled to room temperature. Because the glass, pins and housing materials have different coefficients of thermal expansion (CTE), residual stresses are generated during cool down and subsequent thermal cycling due to the mismatch in thermal strains accumulated at interfaces. If the mismatch causes excessive tensile stresses in the glass, imperfections can lead to cracks that compromise the hermeticity of the seal. A finite element model of a single-pin, concentric glass-to-metal seal is depicted in Figure 1.

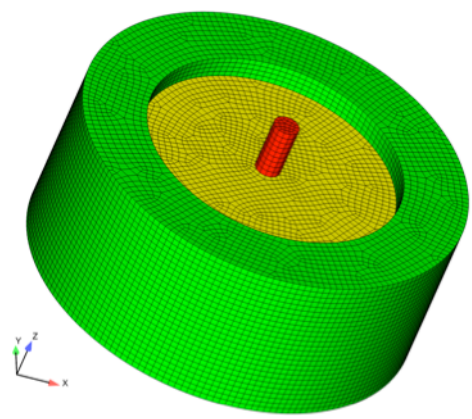

Figure 1 Finite element mesh of concentric, single-pin Glass-To-Metal seal

The choice of materials is an important factor in mitigating the risk of glass fracturing. By design, compression seals use an outer shell material with a CTE that is greater than the glass and a pin CTE that closely resembles or is less than the glass. As such, the glass is subjected to nominal radial compression on cooling that tends to reduce the likelihood of generating high tensile stresses. However, complex geometries still can experience cracking problems. One of the most common material combinations used by Sandia for a compression seal consists of a 304L stainless steel shell, Schott 8061 glass and alloy 52 pins.

Sandia has been designing, analyzing and building glass-to-metal seals successfully for many decades by applying engineering judgment along with a maximum tensile stress failure criterion for the glass. However, as connector designs have evolved to more irregular shapes (e.g., lacking symmetry) and higher pin densities, the challenges of producing crack-free seals have increased. Furthermore, even the more straightforward designs experience unexplained glass fractures occasionally. Sometimes this is observed even when finite element stress analyses have predicted moderate to low tensile residual stresses. Although there are many possible explanations for these events, including anomalous processing and handling issues, all of these point to the need for better understanding and modeling tools to predict quantitatively the

reliability of GTM seal designs. The Brittle Materials Assurance and Prediction Program (BritMAPP) was established to meet the challenges of quantitative mechanics-based failure predictions for brittle materials such as glass, and accurate stress analyses are a prerequisite for any failure predictions. This document proposes a suite of tests to collect data for assessing the accuracy of the residual stress predictions for GTM seal analyses involving S8061 glass and SS304L VAR. The role of alloy 52 pins will need to be considered in a subsequent study.

2 GTM SEAL VALIDATION TESTING

A question that ultimately must be answered is: how accurate are the residual stress predictions for glass-to-metal seals? To address this issue, some experimental quantity must be measured and compared to a model prediction. Although finite element analyses predict the stress tensor at material points, experiments do not directly measure stresses. Stresses may be inferred from collected data (e.g., crack propagation, Raman spectroscopy) but to do so requires additional assumptions that must be confirmed. Other modeling quantities such as deformation and strain are predicted routinely, and indeed, in many circumstances they are directly measureable. However, the deformations and strains in a GTM seal are generated across a broad temperature range. To capture data from the entire glass sealing process and operational environments would require an experimental apparatus capable of surviving and performing precise measurements from about 500 °C all the way down to -55 °C. That is beyond the reach of typical techniques (e.g., strain gauges). Moreover, to make valid comparisons between model predictions and measured data, the GTM seal must survive manufacturing without cracking (i.e., damage altering stress fields), and the test conditions and geometry must be well known to define accurately the initial boundary value problem. A number of potential validation tests have been identified and some preliminary feasibility studies have been conducted. These tests are described in the following sections.

2.1 Indentation Tests to Infer Stresses from Crack Patterns

Indentation methods have been used to infer stresses near the surface of the glass by inducing surface cracks in a glass and comparing crack lengths to patterns generated in a stress-free glass sample (baseline). To investigate the ability of this approach to distinguish stress differences generated by different processing conditions, a concentric GTM seal was studied. Existing samples were used to expedite the investigation. The nominal dimensions of the SS304L shell were 16 mm OD, 10.5 mm ID and 3.5 mm thick. However, since the exact processing history was unknown, it was necessary to reset the cooling history. That was accomplished by reheating the samples to 500 °C and annealing for 30 minutes. Two cooling conditions were investigated, one slow cooled at 0.5 °C/min to room temperature and the second pulled out of the oven for a rapid quench estimated at 100 °C/min to 400 °C. Because this is a compression seal that generated yielding in the shell, subsequent tensile stresses generated on reheating induced circumferential cracking close to the steel-glass interface. The cracking was identical for both the annealed and quenched samples. Since the purpose for this study was only to assess the ability of indentation methods to detect differences in stress state (not to make quantitative predictions), the cracked seals were accepted for indentation.

These disks were indented with a Vicker's diamond indenter at 9.8 N load. Indentations were placed approximately equally spaced from about 500 microns from the interface to the center. The load chosen for this particular glass is such that the crack lengths on the base S8061 glass material are around 80 microns in size. Positive deviations from this crack size in the disk are indicative of local tensile stress, while negative deviations indicate compression. The images of these indentations on one of the disks are shown in Figure 2.

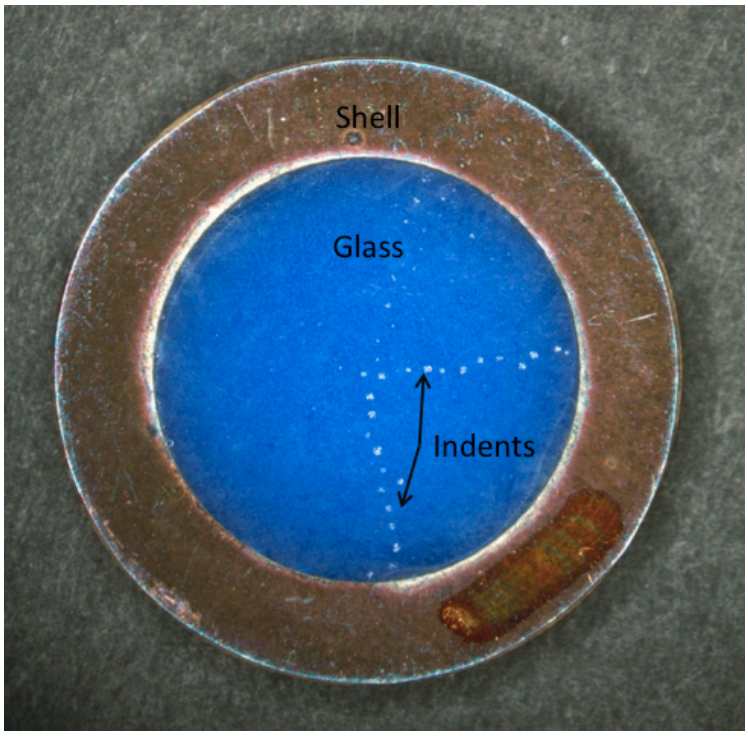

Figure 2 Concentric GTM seal with indentations on surface of the S8061 glass

Measurements of the crack lengths for each indentation were made, considering the following directionality: cracks parallel to shell are termed horizontal, while those perpendicular are called vertical. If the glass in the compression seal was uniformly compressed due to the thermal expansion mismatch with the shell so the radial and circumferential compressive stresses were equal, then the horizontal and vertical crack lengths would be expected to be identical and smaller than the stress-free, baseline glass cracks from indentation. Figure 3 shows higher magnification views of the crack, and the glass microstructure. Pores in the glass are observed, and the locations of the indentations are marked with the yellow arrows. An indent near the shell is shown in the red inset, while one near the center is shown in blue inset. Near the shell, the horizontal cracks on the indent are longer than the vertical ones, indicating either less compression, or perhaps even tension in the radial direction near the shell.

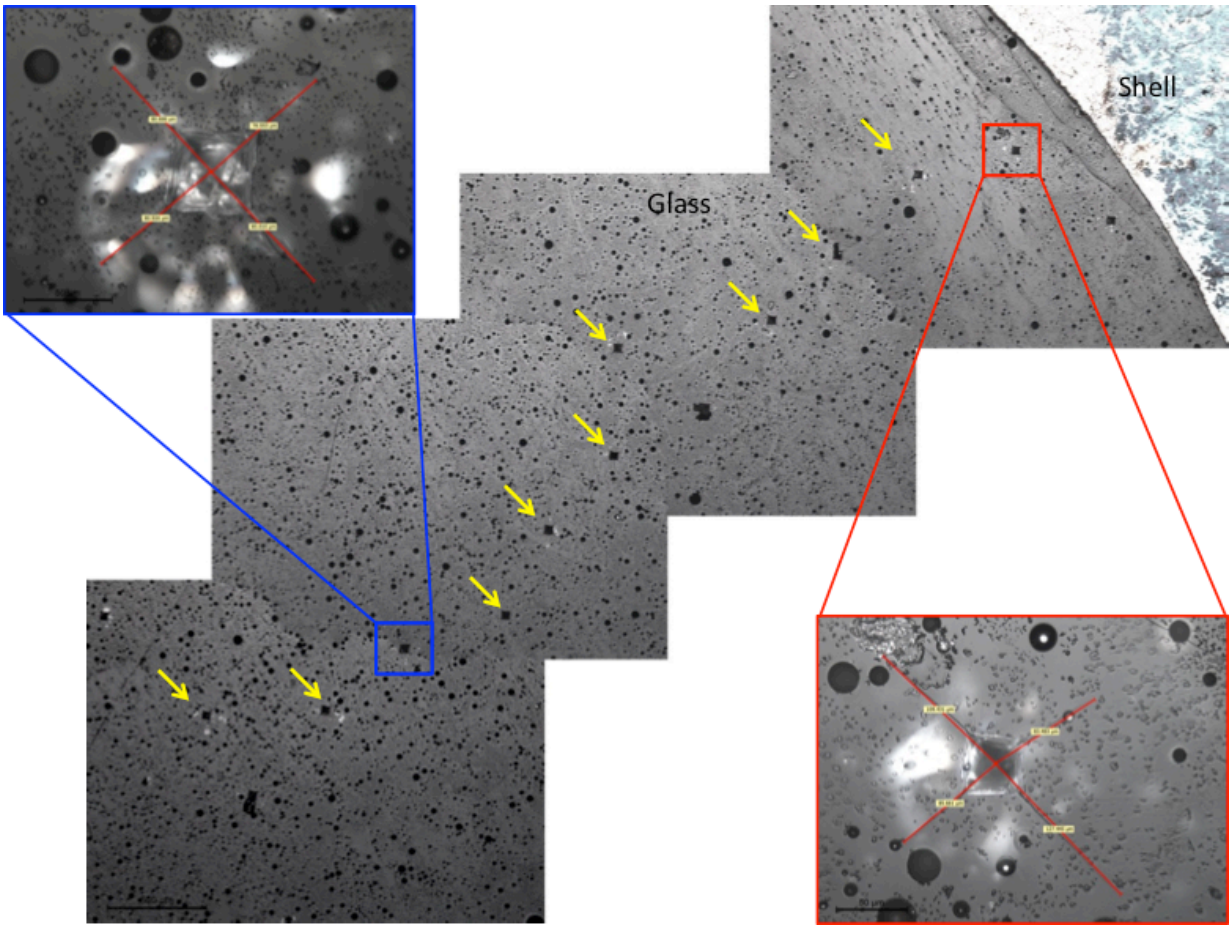

Figure 3 Higher resolution picture of the glass microstructure and cracking at indentations

Figure 4 plots the vertical crack lengths (corresponding to hoop stresses) measured in both the annealed and quenched samples for comparison. Each data point is the average of two indents (four crack lengths). The values of the baseline are also shown. The crack lengths are slightly lower than the baseline close to the center, and there does not appear to be a large difference between the two disks tested. These crack length values are higher than measured in a similar disk which had not been annealed, indicating that some surface compression is relaxed by the annealing treatment. Based on comparison to the baseline, there appears to be only a slight compression in this seal in the circumferential direction.

Figure 5 shows measurements of the horizontal crack lengths (corresponding to radial stresses). While the annealed disk has almost negligible radial compression near the center, the quenched disk appears to have a slightly higher compression, although due to scatter in the data, it is unclear if this can be stated with statistical certainity. Near the glass-steel interface, the crack lengths are significantly higher than the baseline for both disks, indicating that there is a radial

tension in that region. This tension has not been affected by the heat-treatments, although the circumferential crack might have locally relieved the stresses. The extent and influence of porosity is interesting and is under investigation.

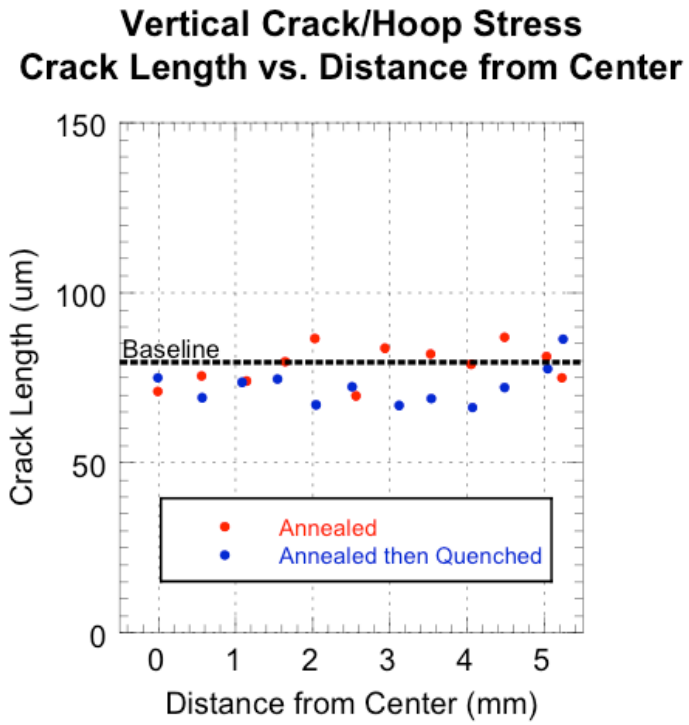

Figure 4 Comparison of vertical cracks generated in indentations on S8061 glass from annealed and quenched concentric GTM seals

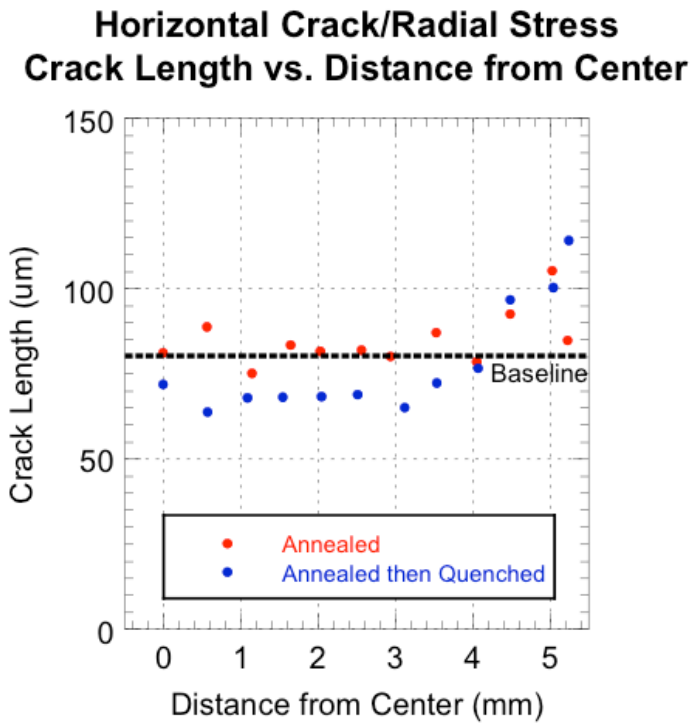

Figure 5 Comparison of horizontal cracks generated in indentations on S8061 glass from annealed and quenched concentric GTM seals

2.2 Measuring Perturbations in the Ambient State of the Concentric Compression Glass Seal

While it is difficult to measure instantaneous and continuous changes in GTM seal deformations during cooling from the high sealing temperatures of nearly 1000 °C, it is possible to measure perturbations about the room temperature residual state. This can be accomplished by instrumenting the seal at ambient conditions and then measuring changes under subsequent well defined thermal-mechanical environments. Nonlinearities in the material behavior (e.g., metal plasticity), will affect the measured response.

For these tests, strain gauges are mounted at three positions 90 degrees apart around the outer shell circumference of the concentric, compression glass seal. A photograph of a strain-gauged seal is provided in Figure 6. The intent is to conduct three types of tests measuring the hoop strain in each strain gauge under three different seal conditions:

1) Under thermal cycling: Here the strains can be measured as the seal is first heated above room temperature (RT) and then cooled to below 0 °C and reheated. Since the SS304L VAR shell is likely to yield on cooling, the data should capture the effects of additional plastic deformation.
2) Boring through the center of the glass: Here a hole is drilled through the center of the glass reducing the radial stiffness of the glass and allowing the SS304L VAR shell to further shrink inward. This will likely produce small changes in strain and may be within

the linear regime of the system. However, it does provide a measure of the relative stiffness.

3) Progressively cutting through the SS304L VAR shell in a radial direction: As the shell is cut, additional plastic deformation will be generated at the tip of the cut which in turn will unload the shell decreasing the hoop strain. The measured response will be affected by the plastic deformation of the shell as well as the interfacial boundary condition.

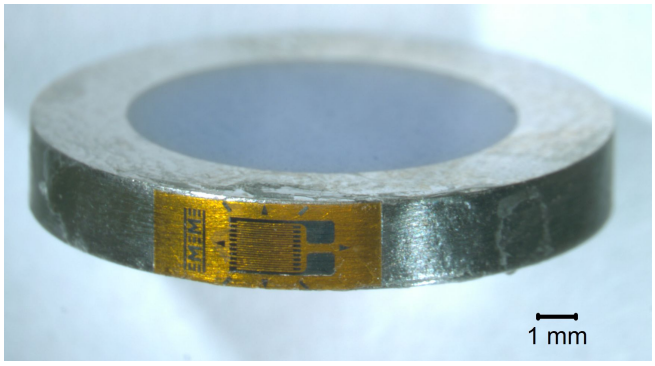

Figure 6 Strain gauge on shell of concentric GTM seal proposed for validation test (thermal cycling, boring through glass or cutting shell)

The sensitivity of the hoop strains to the shell cutting in option #3 were demonstrated clearly by experimenting with the concentric seal described in the previous section. Although this existing SS304L-S8061 seal was from other work and not made with our specific materials according to our specified processing, it was adequate for evaluating the suitability of the test methodology. For comparison purposes, the test was analyzed based on the legacy property set employed routinely for GTM seal analyses. This utilized a thermo-MLEP model for the SS304L and an elastic model with temperature set point of 460 °C for the S8061 glass [see Appendix A]. The thermal residual stresses were computed at RT (20 °C) providing the initial condition for the cutting operation based on the assumption that the glass-shell interface was fully bonded (i.e., continuous mesh). To simulate shell cutting, the shell was partitioned into a number of separate material blocks approximating the width of a saw blade and spanning the radial thickness of the shell as shown in Figure 7. To simulate the hoop strain changes during a cutting operation, the material blocks were deactivated one after another starting from the outer diameter and moving inward. The hoop strain change then was computed from nodal displacement changes taken across the approximate location and length of the strain gauges.

The initial results comparing finite element predictions to the measured strains are shown in Figure 8. Two striking differences are observed. First, the magnitude of the predicted and measured strain changes differ by nearly a factor of three. Second, the shapes of these curves are qualitatively different with predictions being nearly linear while the data are more exponential. Although these analyses were not expected to be quantitative since the materials are different and the processing unknown, the observed differences do suggest that something is being overlooked.

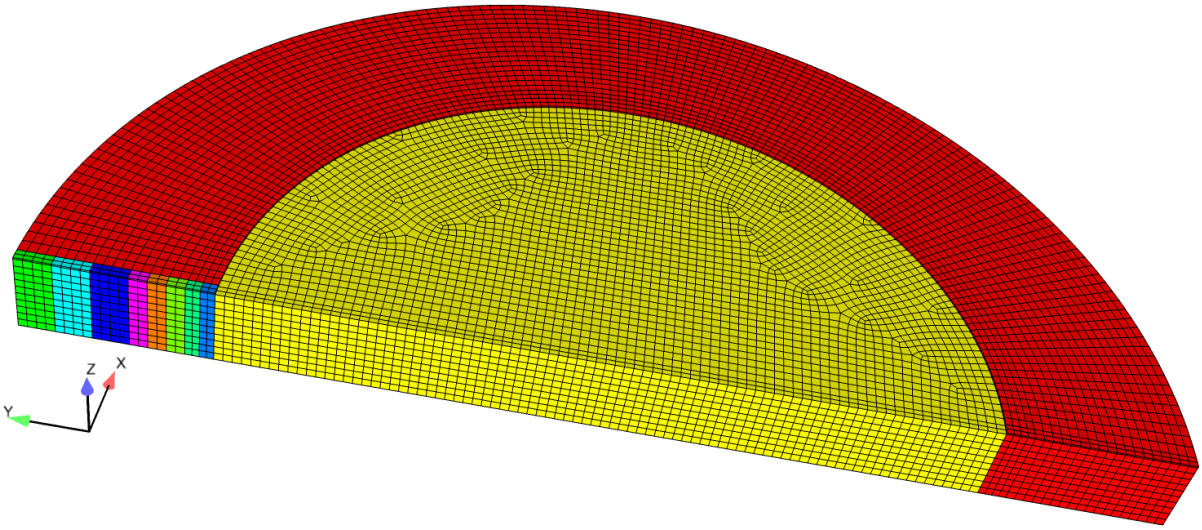

Figure 7 Finite element mesh of concentric seal for cutting

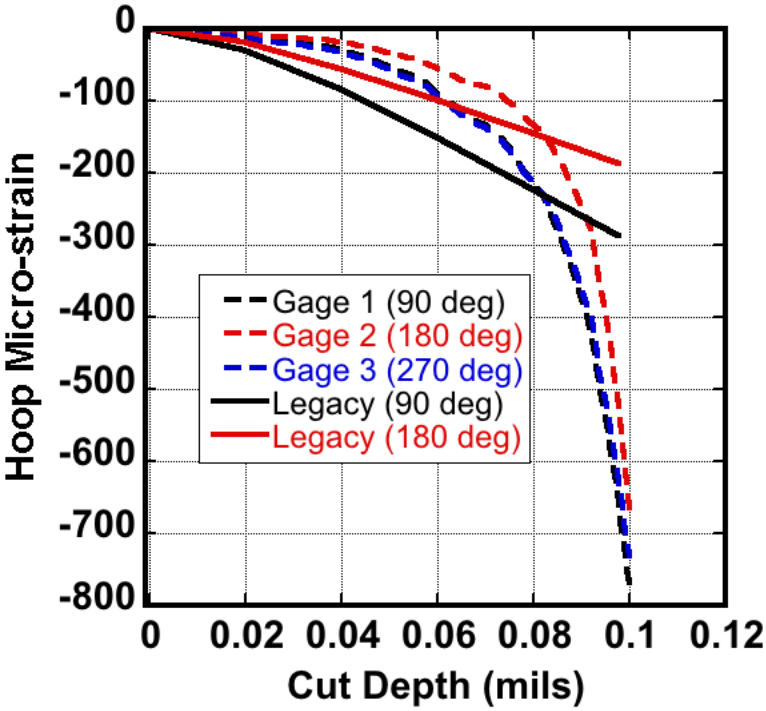

Figure 8 Hoop strain data and FEA predictions obtained using legacy material models to simulate cutting through the shell in a concentric GTM seal

A further consideration of the problem lead to an investigation of the interfacial boundary condition between the glass and the SS304L shell. In a second analysis, contact boundary conditions were adopted with a fiction coefficient equal to 0.60. The results of that analysis are plotted with the hoop strain data in Figure 9. A dramatic change is evident with both the magnitude and shape of the predictions taking on the appearance of the data. This suggests a suitable platform for evaluating the model performance based on variations in boundary conditions (i.e., making seals that are bonded versus those that are not).

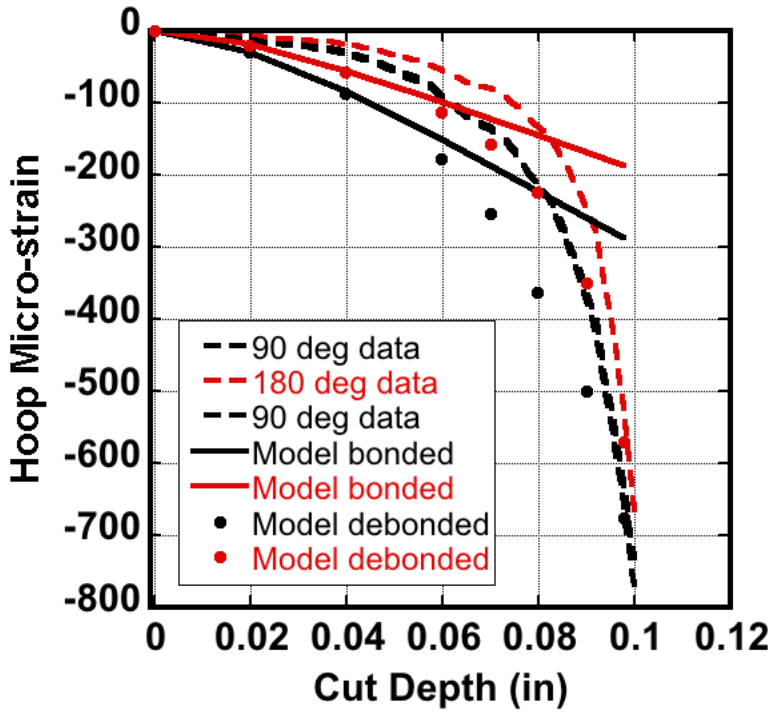

Figure 9 Hoop strain data and legacy predictions for shell cutting process in concentric GTM seal assuming glass-shell contact with a friction coefficient equal to 0.60

2.3 Bi-material GTM Deformations

Because the SS304L VAR and S8061 glass undergo such different thermal strains on cooling from the sealing temperature, GTM bi-material beams curl. If the glass remains crack-free and the interfaces bonded fully, the curvature of the bi-material beams can be measured and used as a metric to assess the fidelity of the finite element modeling and material representations. Moreover, since changes in the cooling rate will affect the thermal strain generated in the glass, this geometry also offers an opportunity to investigate processing affects on the curvature of the bi-material beam.

Bi-material beams were manufactured and the deflected shapes were measured at room temperature. A picture of the visibly deformed beam is shown in Figure 10. The beams were

nominally 50 mm long and 1.845 mm wide. The thickness of the beam layers was found to vary somewhat. In measurements taken at 5 points along the length of a representative beam the metal thicknesses were 603, 616, 625, 642 and 610 microns and the glass thicknesses were 374, 389, 407, 410 and 371 microns.

Figure 10 Picture of bi-material beam made from SS304L VAR and S8061 glass showing deformed shape room temperature (glass on top)

To make some assessment of the sensitivity of the test to material properties, finite element analyses of an "average" bi-material beam were performed using two different property sets. The legacy GTM seal property set was used for one and the newly calibrated thermo-MLEP SS304L VAR model and S8061 SPEC viscoelastic model were used for the other [see Appendix B]. The beam was assumed to be 50.8 mm long and 1.845 mm wide with uniform thicknesses of glass and metal layers defined to be 0.28 mm and 0.619 mm, respectively. In computing the room temperature deflected shape using the legacy properties, the typical assumption was employed making the set temperature (460 °C) the initial stress-free, reference state. For the viscoelastic analysis, care was taken to exploit the fidelity of the model by neglecting the set temperature and starting from a much higher temperature of 600 °C allowing the viscoelastic solidification process to be naturally predicted along with the thermal strain corresponding to a 0.5 °C/min cooling rate. Note the legacy predictions are independent of manufacturing process (i.e., cooling rate) since there is no rate dependence in the legacy material models.

The data measured on two GTM bi-material beams (designated as S16 and S19) are plotted in Figure 11 along with the finite element analysis predictions based on the two property sets with different modeling assumptions. The results are plotted as relative changes in deflection starting from the middle of the beam and moving towards the free end. For these particular analyses, there are observable differences in the predictions. The significance of this, of course, cannot be determined without some understanding of the uncertainties in processing, material properties, geometries, etc. However, this test does provide a viable dataset for studying such variables.

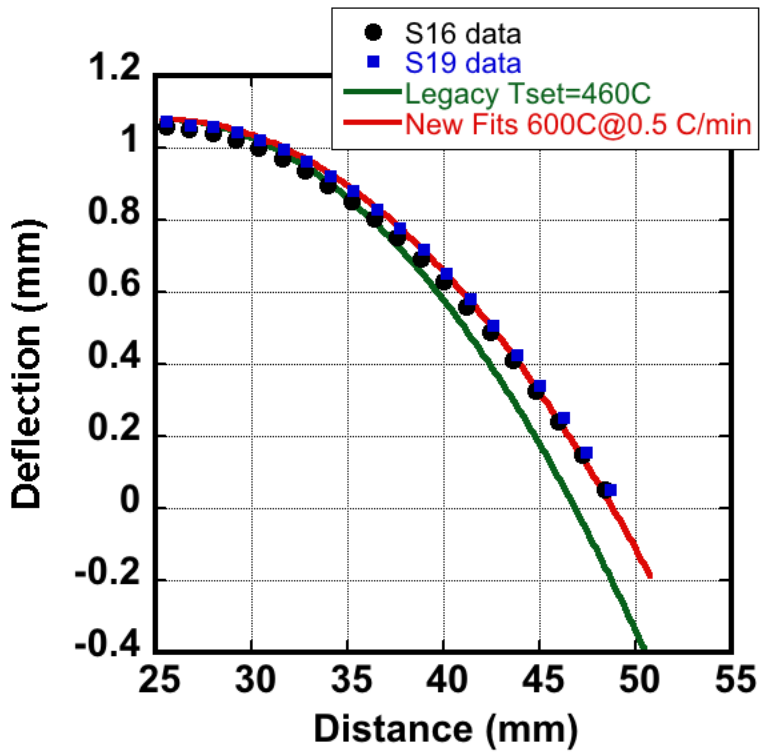

Figure 11 Room temperature deflected shapes from GTM bi-material beams compared to finite element analysis predictions based on two property sets, legacy and newly calibrated thermo-MLEP and SPEC models

Another bi-material geometry that may prove useful for model validation is a variation of the axisymmetric GTM seal concept depicted in Figure 6. In this case, the cylindrical shell (e.g., hollow tube) is chosen to be longer than the thickness of the glass preform. Hence, the glass is recessed substantially from the ends of the tube. As the shell and glass shrink during cool-down from the glass sealing temperatures, the metallic shell will deform around the glass. Since the glass resists the radial shrinkage of the shell, there will be a change in the radius of the deformed shell along the length of the tube from end to end. This is measurable and may be influenced by glass processing schedule.

2.4 Digital Image Correlation (DIC) Methods

To evaluate the possible use of digital image correlation to measure surface strain changes in a GTM seal, the concentric seal discussed in prior sections once again was selected for study. In this case, a white background first was applied to the surface of the seal followed by a speckle pattern with black paint. Before and after pictures of the seal are shown in Figure 12.

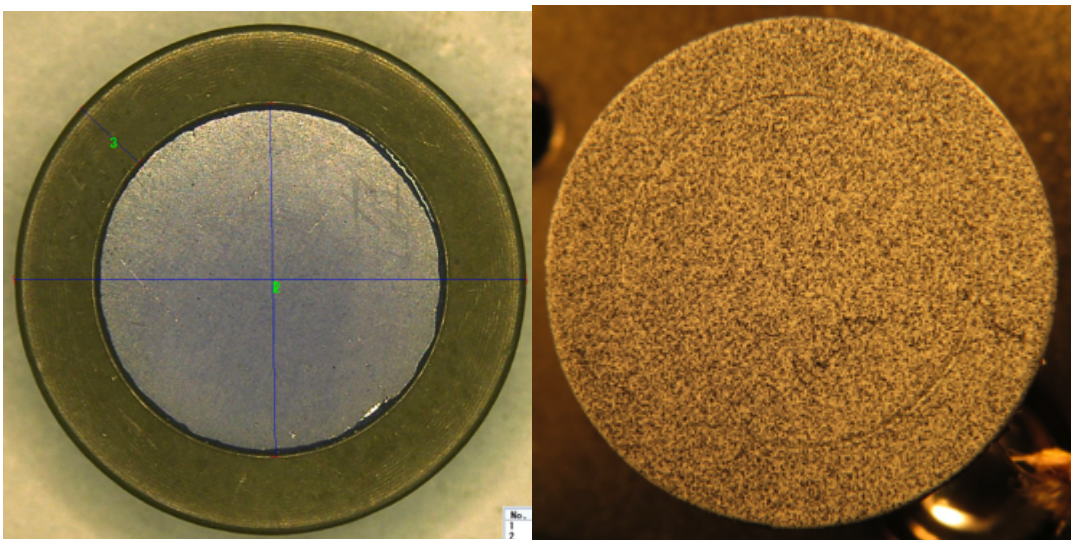

Figure 12 Photographs of concentric seal before and after application of the speckle pattern for the digital image correlation study

The sample was placed on a thermoelectric heating/cooling plate and the temperature was raised from room temperature up to 215 °F (~102 °C) and then cooled to 35 °F (~2 °C). A Canon digital camera with a resolution of 2992x2992 pixels recorded images during the cycle. The relative changes in the positions of the speckle pattern were used to define relative strain changes. Representative painted contours of the first principal strains taken at the 102 °C peak temperature and at 2 °C after cooling are provided in Figure 13 and Figure 14, respectively.

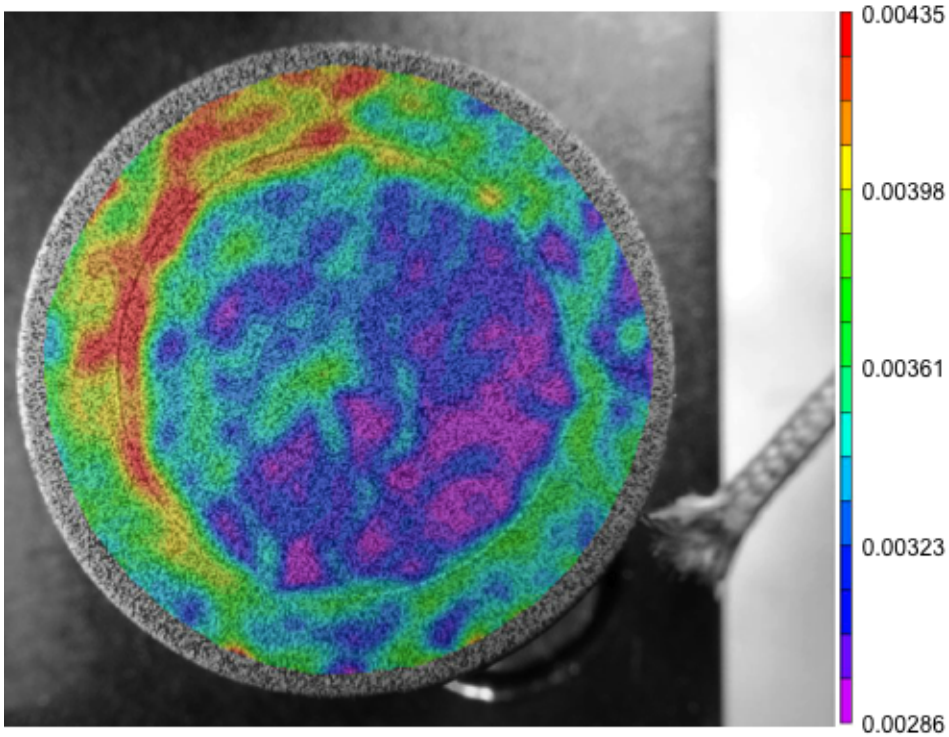

Figure 13 Painted contour of DIC first principal strain change from RT to T=102 °C

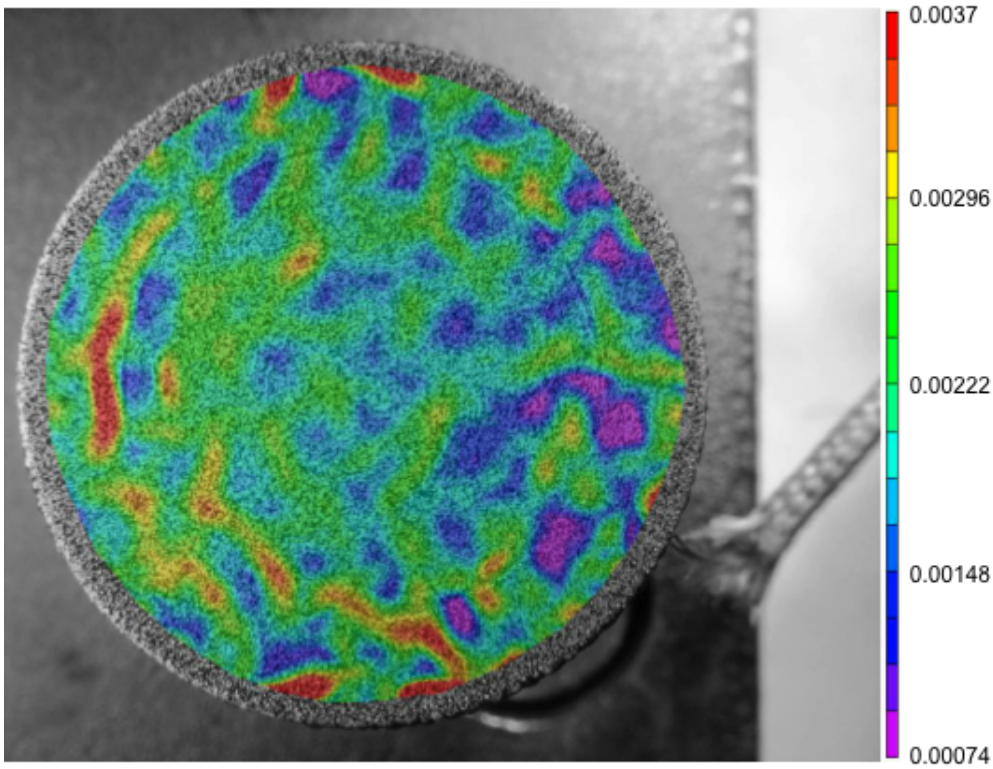

Figure 14 Painted contour of DIC first principal strain change from RT after heating then cooling to 2 °C

Difference in the two strain contours are apparent. Of particular interest is whether the methodology accurately can distinguish strain changes induced by additional plastic deformation. That might be detected by comparing the room temperature results before and after cooling to a much lower temperature if the metal yields further during cooling. The DIC technique is particularly attractive for its ability to compare a spatial distribution in strain. It also might be possible to detect differences resulting from seals that have been processed differently.

3 SOME UNEXPECTED DISCOVERY

In any research and development, there is always some element of discovery that is uncovered. In that regard, this project has been no different. Interestingly enough the discovery comes from both the SS304L VAR and the S8061 glass material behavior. Specifically, it involves how these materials are susceptible to changes over time (e.g., creep). Although we expect this to be true for a viscoelastic glass near the glass transition temperature (T_g), we do not expect to find relaxations occurring 400 °C below T_g and yet we do. In 3-point beam bending under dead loads at room temperature, deflections were measured in the glass over a period of several months. Similarly, when the room temperature stress-strain tests on the SS304L VAR were halted at 2.1% strains (post-yield) and held under constant load for 2.5 hours, the sample creeped by an additional 0.6% strain. Although creep phenomena in SS304L are not new (being known and reported by other researchers), its magnitude and relevance to the GTM seal problem is not common knowledge. Neither of these results was expected and both have implications for long-term aging of GTM seals. Local redistribution of stresses and strain is possible, and the implications for fracture mechanisms is unclear.

This phenomenon of material time dependence at room temperature also may have a significant and unexpected impact on the validation test plan. The material models that initially were identified for GTM seal analyses were not set-up to accommodate room temperature creep. The thermo-MLEP material model is time independent and the SPEC glass model, though indeed viscoelastic, was not calibrated for relaxations this far below T_g. If indeed, the proposed tests are measuring the effects of time-dependent phenomena, then the proposed models may be deficient and additional development will be required. This, of course, does not invalidate the approach. The goal for assessing the accuracy of GTM seal stress predictions still stands. Indeed, the goal becomes even more important for quantifying the effect of the missing physics. The next step will be an assessment of how important this effect is and what to do next. This discussion is provided to acknowledge the issue, raise the awareness of its potential significance and propose a plan forward.

4 SUMMARY

Experiments have been conducted to collect data on the viscoelastic behavior of the S8061 sealing glass and the stress-strain response of SS304L VAR from room temperature to 500 °C in the small strain regime encountered in GTM seals [1]. These data have been used to calibrate a Thermo-Multi-Linear Elastic Plastic (thermo-MLEP) material model for the SS304L VAR and a Simplified Potential Energy Clock (SPEC) viscoelastic material model for the S8061 glass. To assess the accuracy of finite element analyses using these material models to predict stresses and strains in GTM seals, a number of validation experiments have been proposed to collect data for comparison to model predictions. The tests and suitable metrics have been presented and discussed.

In the course of characterizing the material behavior of the SS304L VAR and the S8061 glass, time-dependence has been observed. Specifically, room temperature creep in the post-yield state of the metal and room temperature creep in the glass under a prolonged dead load. Neither of these effects was expected to play a role and yet both have implications for the long-term aging of GTM seals. These findings point all the more to the importance of conducting validation tests to assess the accuracy of proposed modeling strategies while allowing for the need to further enhance the fidelity of material models to include the necessary physics.

6 REFERENCES

[1] Chambers, Robert S., Emery, John M., Tandon, Rajan, Antoun, Bonnie R., Stavig, Mark E. and Clay Newton, Characterization & Modeling of Materials in Glass-To-Metal Seals: Part I, (UUR), SAND2014-0192, Sandia National Laboratories, Albuquerque, NM, January 2014

7 APPENDIX A: LEGACY MATERIAL PROPERTIES

SS304L Adagio Thermoelastic_Plastic Material Model Input Definition (Units: psi, Centigrade)

```
###
### 304L SS Shell
###
begin definition for function thermal_strain_304L
  type is piecewise linear
  ordinate is strain
  abscissa is temperature  ## C
  begin values
    -55.0  -0.00153
     36.6   3.14E-05
     50.1   2.61E-04
    100.1   1.11E-03
    150.1   1.98E-03
    200.1   2.88E-03
    250.1   3.79E-03
    300.1   4.73E-03
    350.1   5.68E-03
    400.1   6.64E-03
    450.1   7.62E-03
    500.1   8.62E-03
    550.1   9.64E-03
  end values
end definition for function thermal_strain_304L

begin definition for function 304_youngs
  type is piecewise linear
  begin values
    -55.0   1.0364
     27.0   1.0000
    110.0   0.8545
    180.0   0.8291
    500.0   0.7636
  end values
end definition for function 304_youngs

begin definition for function 304_poissons
  type is piecewise linear
  begin values
    -55.0   1.00
    500.0   1.00
  end values
end definition for function 304_poissons

begin definition for function 304_yield
  type is piecewise linear
  begin values
    -55.0   35000.0
     27.0   24000.0
    110.0   17000.0
    180.0   14000.0
    500.0   10000.0
  end values
end definition for function 304_yield

begin definition for function 304_hard_-55
  type is piecewise linear
  begin values
    0.0        0.0
    0.0002    400.0
    0.0003   1000.0
    0.0005   2500.0
    0.0008   2750.0
    0.001    3000.0
    0.0015   3300.0
    0.003    4250.0
    0.005    5600.0
    0.008    7750.0
    0.01     9000.0
    0.03    19000.0
    0.05    25500.0
    0.1     40000.0
    0.3    100000.0
    0.4    133000.0
    0.5    155000.0
  end values
end definition for function 304_hard_-55
```

SS304L Adagio Material Model Input Definition (continued)

```
begin definition for function 304_hard_27
  type is piecewise linear
  begin values
    0.0        0.0
    0.0002    730.0
    0.0003   1000.0
    0.0005   1400.0
    0.0008   2000.0
    0.001    2250.0
    0.0015   2750.0
    0.003    3600.0
    0.005    4750.0
    0.008    6500.0
    0.01     7500.0
    0.03    15500.0
    0.05    22000.0
    0.1     36000.0
    0.3     78000.0
    0.4     95000.0
    0.5    109000.0
  end values
end definition for function 304_hard_27

begin definition for function 304_hard_110
  type is piecewise linear
  begin values
    0.0        0.0
    0.0001   1500.0
    0.0002   2000.0
    0.0003   2200.0
    0.0005   2500.0
    0.0008   2800.0
    0.001    2900.0
    0.0015   3200.0
    0.003    4100.0
    0.005    5200.0
    0.008    6800.0
    0.01     7800.0
    0.03    15500.0
    0.05    22000.0
    0.1     36000.0
    0.2     58000.0
    0.3     72000.0
    0.375   79000.0
  end values
end definition for function 304  hard  110

begin definition for function 304_hard_180
  type is piecewise linear
  begin values
    0.0        0.0
    0.0001   2100.0
    0.0002   2700.0
    0.0003   2900.0
    0.0005   3000.0
    0.0008   3100.0
    0.001    3200.0
    0.0015   3350.0
    0.003    4100.0
    0.005    5300.0
    0.008    6750.0
    0.01     7500.0
    0.03    15000.0
    0.05    21000.0
    0.1     35000.0
    0.2     57000.0
    0.3     69500.0
    0.34    72500.0
  end values
end definition for function 304_hard_180
```

SS304L Adagio Material Model Input Definition (continued)

```
  begin property specification for material 304L
    density = 7.4e-4
    thermal strain function = thermal_strain_304L

    begin parameters for model thermoelastic_plastic
      youngs modulus     = 27.5e6    ## psi
      poissons ratio     = 0.264
      yield stress       = 1.0
      beta               = 0.5
      youngs modulus function = 304_youngs
      poissons ratio function = 304_poissons
      yield stress function   = 304_yield
      temperatures       =   -55.0     27.0     110.0     180.0     500.0
      hardening functions = 304_hard_-55  304_hard_27  304_hard_110  304_hard_180
304_hard_180
    end parameters for model thermoelastic_plastic

  end property specification for material 304L
```

S8061 Glass Thermoelastic Adagio Material Model Input Definition (Units: psi, Centigrade)

```
begin definition for function thermal_strain_Schott8061
  type is piecewise linear
  ordinate is strain
  abscissa is temperature
    begin values
      -55.00    -0.000677
       28.95   5.17E-05
       51.20   2.33E-04
      100.92     6.67E-04
      151.08   1.10E-03
      200.95   1.57E-03
      251.10   2.05E-03
      300.90   2.54E-03
      351.20   3.06E-03
      400.93   3.58E-03
      450.88   4.13E-03
      460.00   4.23042e-3    # interpolated
    ##  500.81         5.16E-03
    ##  525.10         5.66E-03
    end values
end definition for function thermal_strain_Schott8061
begin definition for function Schott8061_youngs
   type is piecewise linear
     begin values
        -55.0     1.000
         25.0     1.000
        150.0     0.923
        250.0     0.871
        350.0     0.869
        450.0     0.842
        550.0     0.680
     end values
end definition for function Schott8061_youngs

begin property specification for material Schott8061
 density         =  2.246e-4
 thermal strain function = thermal_strain_Schott8061

  begin parameters for model thermoelastic
    youngs modulus  = 9.8e6  ## psi
    poissons ratio  =  0.21
    youngs modulus function = Schott8061_youngs
  end parameters for model thermoelastic
end property specification for material Schott8061
```

8 APPENDIX B: REVISED MATERIAL PROPERTIES 8/1/14

SS304L Adagio Thermoelastic_Plastic Material Model Input Definition (Units: psi, Centigrade)

```
begin definition for function thermal_strain
  type is piecewise linear
  ordinate is strain
  abscissa is temperature  ## C
  begin values
    -275       -5.81E-03
      28.92    0.00E+00
     499.52    8.71E-03
    1000       0.017886583
  end values
end definition for function thermal_strain

begin definition for function 304L_VARroomTemp
  type is piecewise linear
  ordinate is eqps
  abscissa is yield stress  ## psi
  begin values
    includefile ./TEMP__RT.spline.true.hard.PSI
  end values
end

begin definition for function 304L_VAR100C
  # from smoothed, spline-fit data from B Antoun
  type is piecewise linear
  ordinate is eqps
  abscissa is yield stress       ## psi
  begin values
    includefile ./TEMP__100C.spline.true.hard.PSI
  end values
end

begin definition for function 304L_VAR200C
  # from smoothed, spline-fit data from B Antoun
  type is piecewise linear
  ordinate is eqps
  abscissa is yield stress  ## psi
  begin values
    includefile ./TEMP__200C_1.spline.true.hard.PSI
  end values
end
```

SS304L Adagio Thermoelastic_Plastic Material Model Input Definition (continued)

```
begin definition for function 304L_VAR300C
  # from smoothed, spline-fit data from B Antoun
  type is piecewise linear
  ordinate is eqps
  abscissa is yield stress  ## psi
  begin values
    includefile ./TEMP__300C.spline.true.hard.PSI
  end values
end

begin definition for function 304L_VAR400C
  # from smoothed, spline-fit data from B Antoun
  type is piecewise linear
  ordinate is eqps
  abscissa is yield stress  ## psi
  begin values
    includefile ./TEMP__400C.spline.true.hard.PSI
  end values
end

begin definition for function 304L_VAR500C
  # from smoothed, spline-fit data from B Antoun
  type is piecewise linear
  ordinate is eqps
  abscissa is yield stress  ## psi
  begin values
    includefile ./TEMP__500C_1.spline.true.hard.PSI
  end values
end

begin definition for function constant
  type = piecewise linear
  abscissa = temperature        # temperature C
  ordinate = value              # Unitless Constant
  begin values constant
    -10000.0  1.0
     10000.0  1.0
  end values constant
end definition for function constant
```

SS304L Adagio Thermoelastic_Plastic Material Model Input Definition (continued)

```
begin property specification for material 304L_VAR
  density = 7.8e-03 # approximate 10^6 kg/m^3
  thermal engineering strain function = thermal_strain

  begin parameters for model elastic
    youngs modulus = 29.008E6   ##  200.0e+03  MPa
    poissons ratio = 0.264       # unitless
  end parameters for model elastic

  begin parameters for model thermoElastic_plastic
    beta = 0.5 # kinematic hardening = 0.0; isotropic harening = 1.0
    # temperatures in Celsius:
    poissons ratio = 0.264
    youngs modulus = 24.631128E6  ##       169823. MPa -- RT modulus
    yield stress   = 1.0
    poissons ratio function = constant
    youngs modulus function = constant
    yield stress function = constant
    Temperatures = -55 22 100 200 300 400 500
    hardening functions = 304L_VARroomTemp  304L_VARroomTemp  304L_VAR100C
304L_VAR200C 304L_VAR300C 304L_VAR400C  304L_VAR500C
  end parameters for model thermoElastic_plastic
end
```

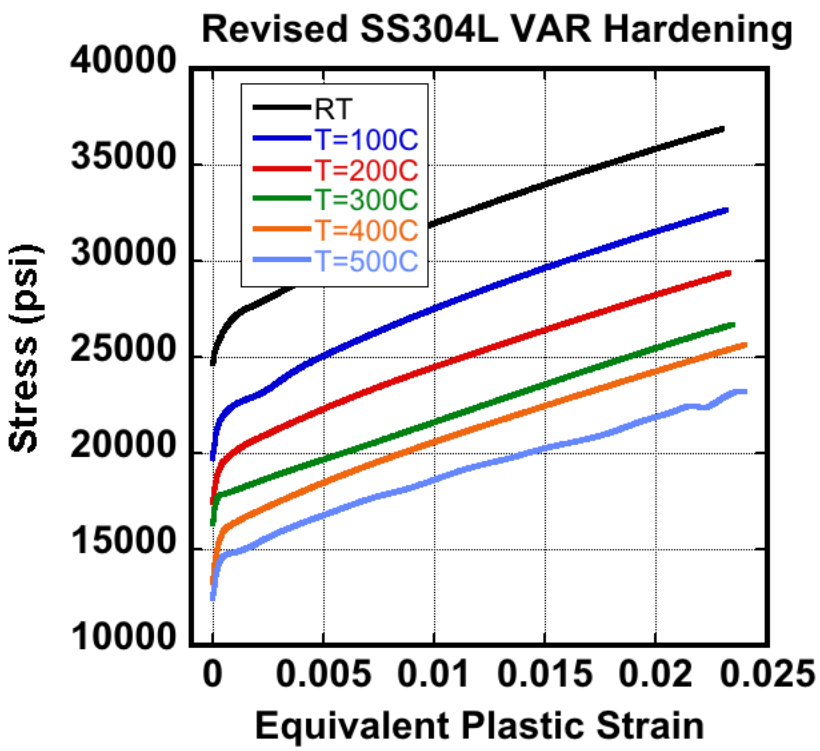

Figure 15 Plots of temperature dependent hardening functions in Adagio thermoelastic plastc model for SS304L VAR

SPEC viscoelastic model parameters

Table 1 SPEC model parameters for Schott 8061 glass

Kg (psi)	4786320 (33 GPa)
dKg/dT (psi/C)	-2973.32 (-20.5 MPa/C)
Keq (psi)	870240 (6 GPa)
dKeq/dT (psi/C)	-855.736 (-5.9 MPa/C)
$volumetric\ CTE, \propto_g\ (ppm/C)$	27
$volumetric\ CTE, \propto_{eq}\ (ppm/C)$	90
Gg (psi)	3618748 (24.95 GPa)
Tref (C)	460
WLF C1	17
WLF C2 (C)	350
normalized bulk relaxation spectrum	$f(t) = e^{(-\frac{t}{30})^{0.3}}$
normalized shear relaxation spectrum	Table 2

Table 2 Prony series coefficients fit to tan delta from second torsion test

g_i	τ_i(sec)
4.24345e-3	1E-8
6.63991e-3	1E-7
6.55255e-3	1E-6
1.41373e-2	1E-5
1.40109e-2	1E-4
2.01033e-2	1E-3
2.66430e-2	1E-2
4.31981e-2	1E-1
5.98391e-2	1E+0
1.46465e-1	1E+1
1.62036e-1	1E+2
2.57094e-1	1.9953E+2
2.39037e-1	1E+3

$$G(t) = [G_g - G_\bowtie] f(t)$$

$$f(t) = \sum_{i=1}^{N} g_i \ \exp\left(-\frac{t}{\tau_i}\right)$$

DISTRIBUTION

1	MS0343	A. Schauer	2610
1	MS0346	D. Peebles	1526
1	MS0346	R. Chambers	1526
1	MS0346	R. Jamison	1526
1	MS0346	K. Ford	1526
1	MS0346	B. Elisberg	1526
1	MS0346	J. Calderone	1526
1	MS0346	M. Neilsen	1526
1	MS0346	J. Holland	1526
1	MS0349	N. Lyon	2614
1	MS0481	M. Neidigk	2224
1	MS0501	M. Craig	2630
1	MS0523	J. Christensen	2633
1	MS0555	T. Cordova	1521
1	MS0557	C. D. Croessmann	1520
1	MS0557	D. Epp	1522
1	MS0557	T. Simmermacher	1523
1	MS0557	S. Klenke	1557
1	MS0557	D. Jones	1558
1	MS0815	J. Johannes	1500
1	MS0840	J. Redmond	1550
1	MS0840	D. Rader	1513
1	MS0840	J. Pott	1555
1	MS0840	H. Fang	1554
1	MS0840	B. Reedlunn	1554
1	MS0840	J. Emery	1526
1	MS0840	L. Tuttle	1555
1	MS0885	D. Wall	1810
1	MS0885	M. Smith	1830
1	MS0886	L. Deibler	1819
1	MS0886	D. Susan	1831
1	MS0887	T. Aselage	1800
1	MS0888	J. McElhanon	1835
1	MS0889	J. Glass	1818
1	MS0889	E. Reedy	1526
1	MS0889	J. Lane	1814
1	MS0889	R. Tandon	1818
1	MS0889	C. Newton	1818
1	MS0889	C. Gibson	1818
1	MS0889	J. Puskar	1831
1	MS0889	J. Rodelas	1831
1	MS0889	B. Boyce	1831
1	MS0958	M. Kelly	1833

1	MS0958	M. Stavig	1835
1	MS0958	J. Kropka	1835
1	MS0958	N. Wyatt	1835
1	MS0959	S. Dai	1833
1	MS1135	R. Watkins	1532
1	MS1318	T. Trucano	1440
1	MS1349	W. Hammetter	1815
1	MS1349	K. Ewsuk	1815
1	MS1349	S. Reed	1815
1	MS1349	D. Bencoe	1815
1	MS1411	A. Sun	1814
1	MS9035	P. Spence	8250
1	MS9042	M. Chiesa	8259
1	MS9042	J. Ostien	8256
1	MS9042	B. Antoun	8256
1	MS0899	Technical Library	9536 (electronic copy)

Sandia National Laboratories